

## Rochester Institute of Technology RIT Scholar Works

---

Presentations and other scholarship

Faculty & Staff Scholarship

---

3-15-2006

# Evanescent Eave Imaging in Optical Lithograpy

Bruce W. Smith

*Rochester Institute of Technology*

Yongfa Fan

*Rochester Institute of Technology*

Jianming Zhou

*Rochester Institute of Technology*

Neal Lafferty

*Rochester Institute of Technology*

Andrew Estroff

*Rochester Institute of Technology*

Follow this and additional works at: <https://scholarworks.rit.edu/other>

---

### Recommended Citation

Bruce W. Smith, Yongfa Fan, Jianming Zhou, Neal Lafferty, Andrew Estroff, "Evanescent wave imaging in optical lithography", Proc. SPIE 6154, Optical Microlithography XIX, 61540A (15 March 2006); doi: 10.1117/12.657322; <https://doi.org/10.1117/12.657322>

This Conference Paper is brought to you for free and open access by the Faculty & Staff Scholarship at RIT Scholar Works. It has been accepted for inclusion in Presentations and other scholarship by an authorized administrator of RIT Scholar Works. For more information, please contact [ritscholarworks@rit.edu](mailto:ritscholarworks@rit.edu).

# Evanescient wave imaging in optical lithography

Bruce W. Smith, Yongfa Fan, Jianming Zhou, Neal Lafferty, Andrew Estroff  
Rochester Institute of Technology, 82 Lomb Memorial Drive, Rochester, New York, 14623

## ABSTRACT

New applications of evanescent imaging for microlithography are introduced. The use of evanescent wave lithography (EWL) has been employed for 26nm resolution at 1.85NA using a 193nm ArF excimer laser wavelength to record images in a photoresist with a refractive index of 1.71. Additionally, a photomask enhancement effect is described using evanescent wave assist features (EWAF) to take advantage of the coupling of the evanescent energy bound at the substrate-absorber surface, enhancing the transmission of a mask opening through coupled interference.

**Keywords:** Evanescent wave lithography, solid immersion lithography, 193nm immersion lithography

## 1. INTRODUCTION

The pursuit of optical lithography at sub-wavelength dimensions leads to limitations imposed by classical rules of diffraction. Previously, we reported on the use of near-field propagation in the evanescent field through a solid immersion lens gap for lithography at numerical apertures approaching the refractive index of 193nm ArF photoresist.<sup>1</sup> Other groups have also described achievements with various configurations of a solid immersion lens for photolithography within the refractive index limitations imposed by the image recording media, a general requirement for the frustration of the evanescent field for propagation and detection.<sup>2-4</sup> We have extended the resolution of projection lithography beyond the refractive index constraints of the recording media by direct imaging of the evanescent field into a photoresist layer with a refractive index substantially lower than the numerical aperture of the imaging system.

In addition to the potential enabled through the detection of the evanescent field at the image plane, coupling of the surface bound evanescent field at the photomask object plane can lead to a near field enhancement of the far field image. We also report on these two phenomena and their applications here.

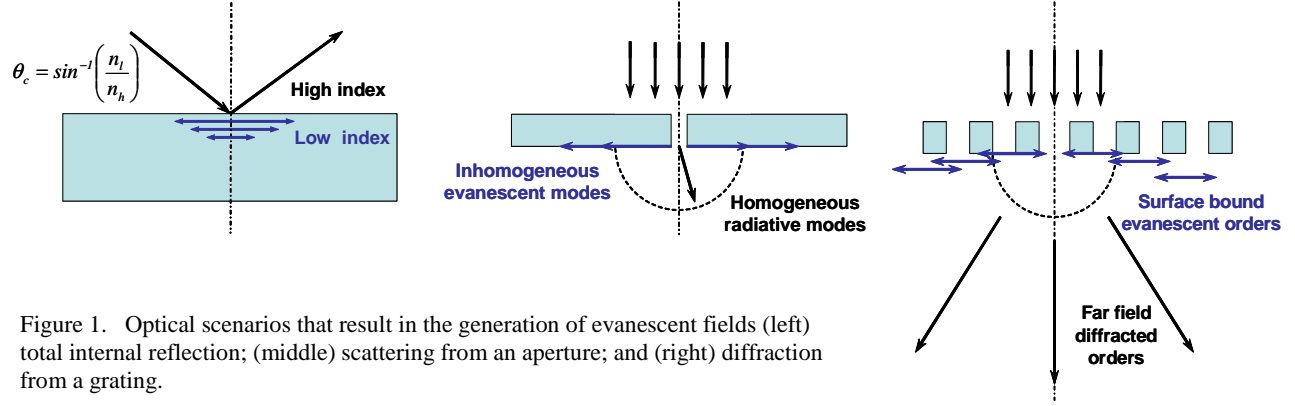
### 1.1 Evanescent waves at a media interface

Evanescient waves are by classification elusive, as they are defined by their rapid decay and ability to escape measurement. Newton was the first to uncover their existence in a well known experiment where he contacted the facet of a prism illuminated under total internal reflection with a lens to discover a luminous region of propagation that extended beyond the contact region of the optical components. This first observation of an evanescent field under the frustration of a high refractive index media was not quantified until the early part of the twentieth century. The effect was not applied toward optical devices for several decades. The phenomenon is now the basis of several important technologies including guided optics, waveguides, fiber optic couplers, internal reflection spectroscopy, tunneling optical microscopy, and near-field microscopy, among others.

An evanescent field can be generated several ways. Figure 1 shows three examples of optical situations for the creation of an evanescent effect, namely total internal reflection at the interface between two media; the scattering or near-field diffraction from a small aperture; and the diffraction from a collection of apertures or a grating. For the case of total internal reflection, illumination of the interface between two media of different refractive indices will lead to homogeneous propagation of radiation at angles below the critical angle, defined as:

$$\theta_c = \sin^{-1}\left(\frac{n_l}{n_h}\right) \quad (1)$$

where  $n_l$  and  $n_h$  are the refractive index values for the media of low and high refractive index respectively. At these angles, radiation will obey Snell's law of refraction with conventional radiometric properties, including the inverse square loss of irradiance and extinction based on the absorptive properties of the medium. At angles beyond critical,



radiation will no longer be homogenous but instead inhomogeneous, with rapid diminishment driven by the disparity of the refractive indices and the angle of illumination. This evanescent field does not propagate in the classical sense to obey refractive, diffractive, or reflective behavior but instead decays rapidly within a sub-wavelength scale as:

$$A(z) = e^{-\left(\frac{2\pi n_h}{\lambda} \left[ \sin^2 \theta - \left(\frac{n_l}{n_h}\right)^2 \right]^{1/2} + \alpha\right) z} \quad (2)$$

where  $n_h$  and  $n_l$  are the refractive indices of the media that the evanescent is propagating from and into, respectively, and  $\theta$  is the angle of illumination in the first media.

## 1.2 Evanescent waves at a small opening

In the case of the illumination of a small aperture in an opaque screen, it is well understood that the far-field diffraction pattern propagates as the Fourier Transform of the opening. As the aperture size is decreased, the propagating “point spread function” possesses a correspondingly larger aperture of propagation. As the aperture is made smaller than half-wavelength, the corresponding wave vector in the direction of propagation ( $z$ ) falls to zero and then becomes purely imaginary.<sup>5</sup> This energy does not propagate but remains bound to the surface or medium interface. In essence, the lowest spatial frequency of the aperture (the DC component) is transmitted and all higher frequencies remain in the  $z$ -plane where no structural detail of the aperture is propagated.

For a collection of sub-wavelength apertures, or a grating, the far field Fraunhofer diffracted energy is determined classically as:

$$\sin \theta_m = \frac{\pm m \lambda}{p} \quad (3)$$

where  $m$  is the far field diffraction order and  $p$  is the grating pitch. As diffraction order angles reach unity, they are described as evanescent or surface bound. This is a near field implication to the far field effect as the evanescent field never escapes the sub-wavelength region of the grating surface for propagation to the far field. As a grating pitch approaches the illuminating wavelength (irregardless of aperture size or spacing), only the zero order escapes to the far field. All other orders are confined to the near field as evanescent to the surface, leading to what can be referred to as a “zero-order grating”.<sup>6</sup>

## 2.0 FRUSTRATED TOTAL INTERNAL REFLECTION

When illuminated at an angle beyond critical, TIR results with evanescent wave decaying according to Equation 2. The decay continues with distance and would theoretically lead to the existence of the evanescent field at any location,  $z$ . More practically, the penetration depth is defined as:

$$d_p = \frac{\lambda}{2\pi\sqrt{n_h \sin^2 \theta - n_l^2}} \quad (4)$$

where the energy in the evanescent field drops to a value of  $1/e$  from that at  $z=0$ , defining its confinement to the sub-wavelength values. Polarization plays a large role in the nature and magnitude of the energy at the media interface. For transverse electric polarization (TE), the evanescent field is transverse to the direction of propagation while for transverse magnetic (TM) polarization, separable components have a  $\pi/2$  phase difference.<sup>7</sup>

Though the amplitude of the evanescent electric field decreases with distance, the average energy in the field over time is zero. Direct detection is therefore not possible unless the field is perturbed in some way to force it into propagation. Newton achieved such perturbation through frustration of the evanescent field with a media of higher index, allowing for the escape and propagation of energy from illumination at angles beyond critical. Figure 2 shows frustrated total internal reflection (FTIR) and how illumination resulting in an evanescent field in a gap between two media can be transformed into a propagating field. When a third frustrating media is introduced to form a second interface, fields evanescent in the gap escape and propagate if the refractive index ( $n_f$ ) is:

$$n_f \geq n_{upper} \sin \theta_{upper} = NA \quad (5)$$

where  $\sin \theta$  is the illumination angle in the incident media and  $NA$  is the invariant numerical aperture. The emerging wavefront exits from the interface with the same propagation angle and polarization as the incident wave. The amplitude of the field at this interface is dependent on the wavelength, the incidence angle, and the gap, and has been described by Salomon et al.<sup>8</sup>

The effect of FTIR was first quantified by Selenyi in 1913 by coating the top face of a hemispherical prism with a fluorescing material and illuminating through it with a large angle source, as shown in Figure 3. Through the detection of the intensity escaping the prism at angles greater than critical, it was evident that an evanescent wave must be present in the fluorescing film to further frustrate and propagate out of the interface.<sup>9</sup> The FTIR effect is also the basis of the solid immersion lens, used in applications including optical storage and solid immersion microscopy.<sup>10</sup> It is shown schematically in Figure 4, where a small gap, most commonly air, is controlled between a hemispherical last optical element and a substrate. At near field distances, the evanescent field in the gap resulting from TIR illumination is propagated by the frustration from the higher index substrate. Extension of this approach to lithography has also been described.<sup>1,2</sup>

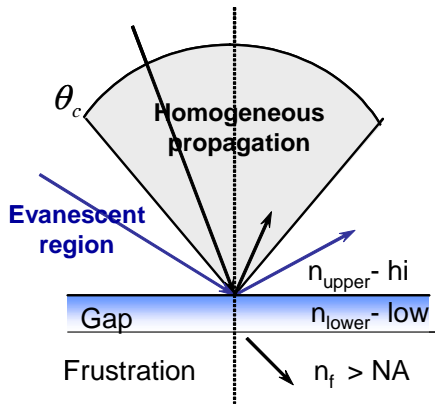


Figure 2. Frustrated total internal reflection (FTIR) of an evanescent field into a media with refractive index larger than the numerical aperture of the propagating wavefront.

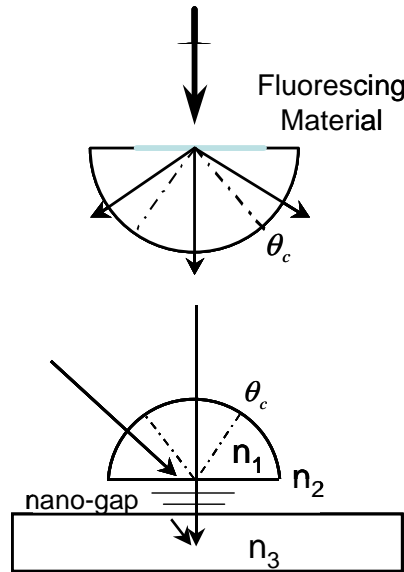


Figure 3. The principle of the Selenyi experiment detecting energy from an evanescent field within a fluorescing material through propagation.

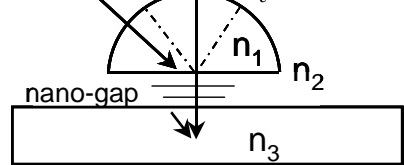


Figure 4. Schematic of a solid immersion lens with an air gap in the near field region.

### 3.0 LITHOGRAPHY USING FTIR

We have constructed an experimental setup for lithographic patterning of frustrated TIR using projection interferometry at 193nm, as shown in Figure 5. The system is comprised of a Lambda Physik Optex Pro ArF excimer laser with a TROM spectral line narrowing to achieve a temporal bandwidth of 5-10pm and a spatial coherence length of 0.25-0.50mm. The beam is further conditioned for polarization and uniformity control using a Rochon MgF<sub>2</sub> polarizer and a 5X fused silica beam expander of a Galilean design. A fused silica phase grating with a lateral pitch dimension of 600nm and a depth corresponding to a phase shift of  $\pi$  is used to split the beam into two orders (+1 and -1) for use in a Talbot interferometry configuration. Any residual on-axis zero-order transmission through the mask is obscured using a small beam blocker. Below the grating mask are a pair of aluminum coated turning mirrors to direct the grating orders toward a coupling prism for their recombination and interference. The prism is equilateral, cut from hexagonal crystalline sapphire (aluminum oxide), with opposing facets coated with a quarter wave thickness of magnesium fluoride for anti-reflection at 193nm. The prism is placed within an assembly which allows for alignment and also the insertion of small silicon wafer samples in close contact to the prism surface normal to the optical axis. The assembly allows for clamping of the silicon sample to allow for a sub-wavelength gap, which can be gauged using reflection measurement techniques and correlation to the intensity values expected from Equation 2. Silicon wafer samples were coated with approximately 70nm of poly acrylate 193nm photoresist material (JSR 1941J, with a refractive index of 1.71) over a bottom anti-reflective coating (Brewer ARC29A).

Imaging results are shown in Figure 6. The system was set up for imaging with three situations: 1.42 NA for 34nm half pitch; 1.60 NA for 30nm half-pitch, and 1.66 NA for 29nm half pitch. Under each of these conditions, the air gap between the sapphire prism and the resist media was on the order of 10-15nm. The photoresist media with a refractive index of 1.71 leads to the frustration of the evanescent wave in the gap, allowing for the propagation, detection, and recording of the image into the photoresist. It would be expected that the condition for 1.66 NA would represent the limitation of the system, since the angle of the re-propagated electric field in the photoresist is nearly 80 degrees [ $\sin^{-1}(1.66/1.71)$ ].

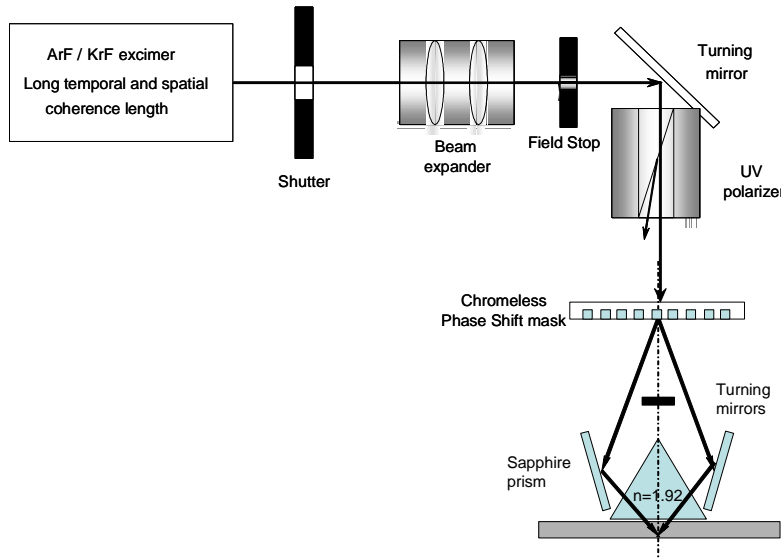


Figure 5. Schematic of the sapphire imaging system used for solid immersion lithography (SIL) and evanescent wave lithography (EWL).

### 4.0 EVANESCENT WAVE LITHOGRAPHY (EWL)

As the numerical aperture of the system is increased further and beyond the refractive index of the photoresist, the ability to perturb the evanescent field through frustration is removed as would seem the ability to detect or record an image. Figure 7 shows the results of imaging under the configuration of numerical aperture of 1.85. Since the same photoresist is utilized (with a refractive index of 1.71) and imaging of 26nm features has been accomplished, it is evident that frustration of the evanescent wave is not necessary for propagation and collection. We refer to this as evanescent wave lithography (EWL). Though the result appears as a simple extension of the solid immersion

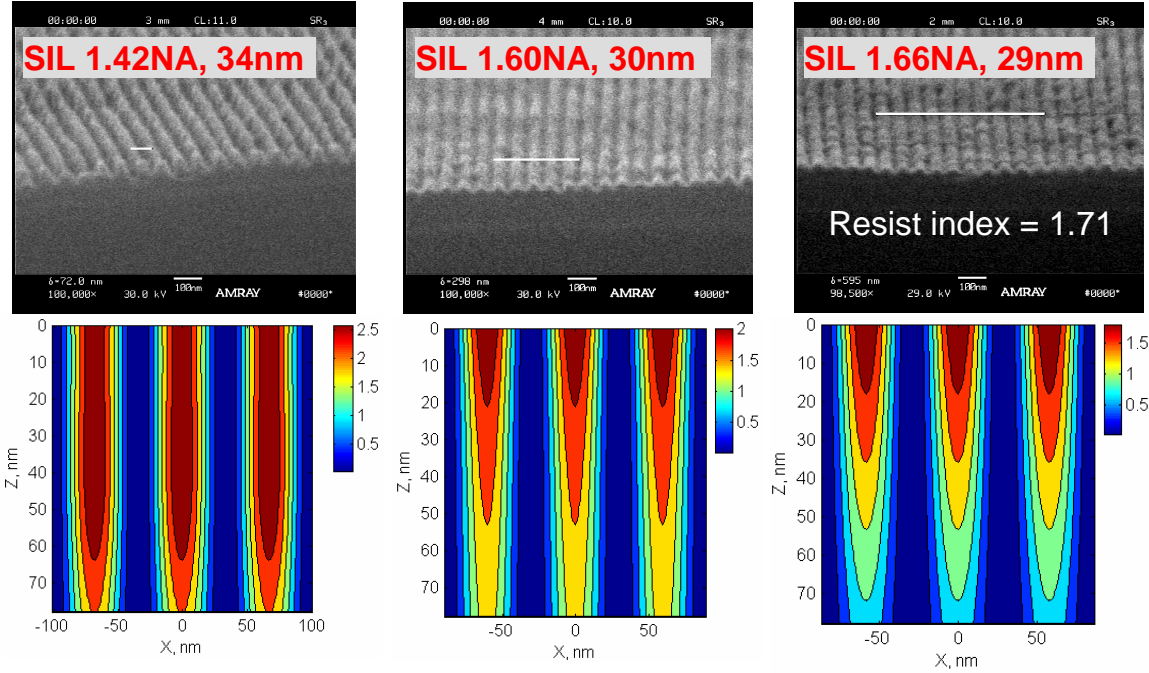


Figure 6. Solid immersion lithography results using the sapphire imaging system (left) 1.42NA for 34nm half-pitch imaging; (middle) 1.60NA for 30nm half-pitch imaging; and (right) 1.66NA for 29nm half-pitch imaging in 78nm photoresist along with ILSim simulations.

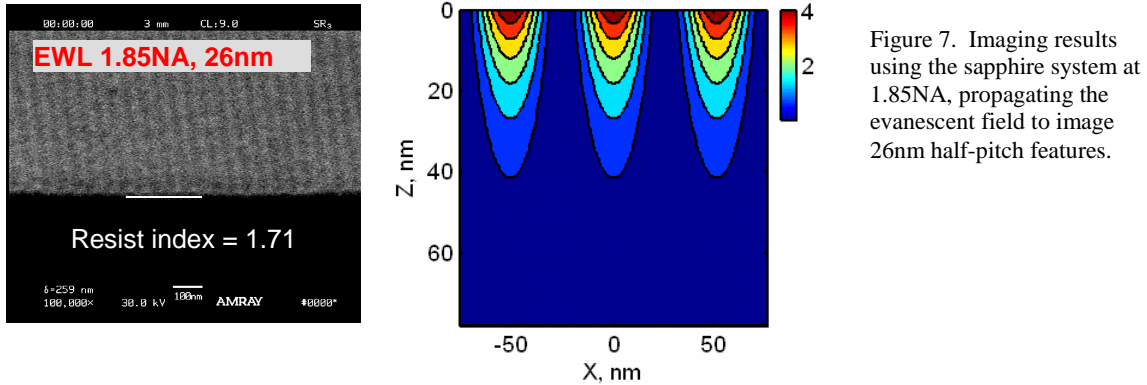


Figure 7. Imaging results using the sapphire system at 1.85NA, propagating the evanescent field to image 26nm half-pitch features.

lithography (SIL) cases of Figure 6, this extends beyond FTIR limits by imaging the evanescent wave itself. Since the average evanescent field energy is zero, perturbation is caused by means other than high index frustration. We postulate that since two propagating coherent beams are used to create corresponding but separate evanescent fields, mutual evanescent wave perturbation is carried out within the photoresist film, leading to propagation and interference that follows exponential decay. These evanescent waves have the same frequency as the propagating wave and a finite phase shift with respect to each other. Their interference results in a sinusoidal distribution of intensity, with a resulting pitch determined by the vacuum wavelength ( $\lambda_v$ ) and the NA invariant of the imaging condition, as  $\lambda_v/\text{NA}$ , which would be calculated for interference of two propagating wavefronts. Conceptual reconciliation of an NA for an angle greater than  $\pi/2$  is difficult, since the refractive index does not change. A more manageable description of the phenomena is a corresponding wavelength scaling, as necessitated to conserve an angle no greater than  $\pi/2$ .

A set of exposures was carried out at numerical aperture values of 1.75 and 1.85 with two gap conditions to study the propagation effect of EWL into a photoresist film. For one case, an air gap of 10nm separated the sapphire and photoresist media while a second case comprised an added top-coat layer over the photoresist to act as an additional separation layer. The top-coat layer was a base soluble transparent polymer (JSR TCX014) with a refractive index of 1.54, spin coated to a thickness of 35nm. A vector-based interference lithography simulator, ILSim<sup>11</sup> was used to predict

the image intensity within the photoresist for both numerical apertures at both gap conditions. Results are plotted in Figure 8, along with resist image results from the sapphire EWL set-up. The evanescent wave intensity is plotted normalized to the energy at the top of the resist film. In order to correlate these values to resist image results, the required exposure dose for each case was similarly normalized and calibrated to this same energy value. Since the decay of the evanescent field results only in a loss of field amplitude, there is no loss of modulation in the images, other than that which may be a result of scatter in the image system. These results also give insight into the scale of the tolerable gap for EWL if it were to be employed in a moving stage situation. If gap control in the 20-60nm range could be maintained, which can be achieved with current solid immersion lens systems, a lithography approach using this principle could become manageable. Though the image depth into the photoresist is shallow, in the range of the penetration depth ( $d_p$ ), methods of top-surface imaging could be employed to transfer these patterns for delineation of a thicker underlying film.<sup>12</sup> A practical and immediate application of EWL is for the exploration into the extendibility of optical lithography into and beyond 32nm patterning generations.

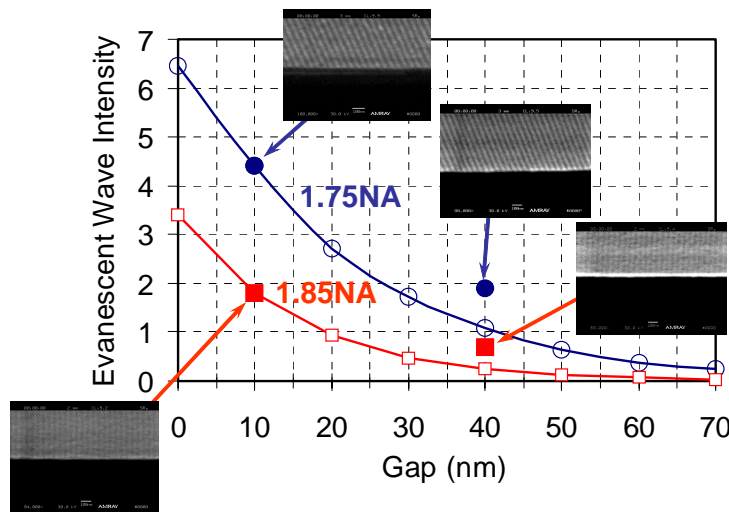


Figure 8. Field intensity plot for propagation through a gap of increasing thickness for 1.75NA and 1.85NA, together with exposures made in photoresist.

## 5.0 EVANESCENT LITHOGRAPHY AT THE PHOTOMASK AND EWAF

The scatter distribution of a sub-wavelength aperture includes energy propagating into free-space as well as surface bound evanescent energy. This total surface energy is the superposition of evanescent waves emanating from the aperture. The diffracted field of a zero-order grating includes surface bound evanescent energy as a collection of the evanescent waves emanating from each aperture. The question arises as to whether these evanescent waves can interfere in such a way as to create a composite superpositioning, resulting in constructive and destructive effects, as does the interference of a conventional propagating electric field. Leviatan<sup>13</sup> investigated whether the diffraction of evanescent waves could lead to propagating waves just as diffraction of plane waves can generate evanescent waves. By studying the effect of the lateral separation of two sub-wavelength apertures separated in the near field for microwave application, it was discovered that the lateral shifting between these apertures could lead to a harmonic coupling resonance with maximum enhancement at regular spacing intervals. Lezec and Thio<sup>14</sup> presented an expansion of the phenomena to describe the enhancement observed as an opening in a metal film over glass is surrounded by periodic grooves. These periodic sub-wavelength grooves create evanescent waves that are confined to the surface of the metal film. A composite diffracted evanescent wave is formed as the full surface wave energy traveling toward the opening is a superposition of these surface waves.

We have expanded these concepts for application to a photomask and describe the enhancement using Evanescent Wave Assist features (EWAF). As mask dimensions approach the sub-wavelength scale, the surface-confined evanescent energy needs to be considered together with the propagation of diffracted energy into free space. The portion of the illuminated energy that becomes evanescent increases as mask features shrink. The



evanescent effect is already important for the 45nm node, which correlates to 180nm (or  $0.93\lambda$ ) for a 4X reduction mask and assist features approach sizes as small as 60nm (or  $0.31\lambda$ ).

To study the effect that a composite diffracted wave effect could contribute to the behavior of a photomask, a series of assist structures, called evanescent wave assist features (EWAF) were designed for simulation using a finite-difference time-domain model solution to the Maxwell equations.<sup>15</sup> Figure 9 shows the layout of a single space opening in a photomask, flanked by grooves patterned into the mask substrate. An absorber layer covers the grooves, burying them and preventing any propagation through the film. When the grooves and their period are sub-wavelength, a zero-order diffraction grating is formed, forcing all other energy to be evanescent in the glass-thin film interface. As the period becomes larger than the illuminating wavelength, the evanescent field decreases but is still present as long as the groove size remains sub-wavelength. Under plane wave illumination, each groove launches an evanescent wave which will travel along this interface perpendicular to the main space opening. The amplitude of these evanescent waves decreases exponentially with distance but they will interfere with each other during their travel. If added constructively, the total composite field can increase with each successive interaction. If this coupling wave then encounters an opening, the amount of energy that propagates through that opening is modulated based on the phase interference between the composite fields. The modulation of the amplitude through the opening can be determined as<sup>13</sup>:

$$A(\lambda) = \left( 1 + 2 \sum_{j=1}^N \frac{\alpha d}{jP} \cos \left( \frac{2\pi}{\lambda} n_{eff} P + \frac{\pi}{2} \right) \right)^2 \quad (6)$$

where  $a$  is the amplitude of the evanescent wave launched at each groove relative to the illuminated energy,  $p$  is the period of the groove spacing,  $d$  is the width of the groove, and  $n_{eff}$  is the effective refractive index along the interface.

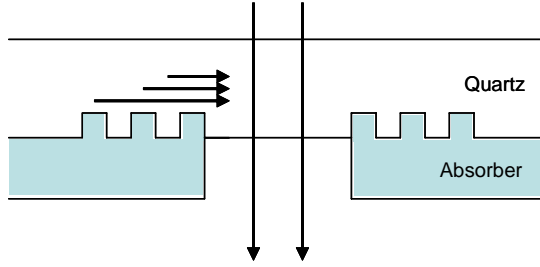


Figure 9. Schematic of evanescent wave assist features (EWAF) to enhance the near field transmission of a nearby opening.

Figure 10 shows the result of the analysis. A 180nm opening was evaluated on a 862nm pitch (45nm and 215.5nm respectively at the image plane). EWAF sizes of 62nm x 62nm were used to flank the opening at  $N = 0, \pm 1, \pm 2, \pm 3$ , and  $\pm 5$  pairs. A 90nm chromium film was used as the absorber and simulations were carried out for 193nm wavelength. The results show the near field electric field energy through the main feature opening, which is highlighted with a constant intensity contour at the center of each case. The case where one pair ( $N = \pm 1$ ) shows an increase in transmitted intensity compared to  $N = 0$ , as does  $N = \pm 2$  and  $N = \pm 5$ . At  $N = \pm 3$ , however, the total transmitted intensity through the opening decreases slightly through destructive interference of the coupled evanescent wave. After the full composite field passes through the opening, radiation is diffracted as would be predicted based on the propagating homogeneous field alone. Figure 11 shows the intensity in the opening for the best case ( $N = \pm 2$ ) compared to the  $N = 0$  baseline case. The increase in the near field intensity at the center of the opening is nearly 17% while the energy is confined with a 20% decrease in effective sizing. The effects modeled here cannot be explained by phenomena other than the evanescent field. Other explanations of transmission enhancement in sub-wavelength hole arrays in metal films have attributed the effect to surface plasmons. This effect would not be predicted based on the FDTD modeling and would be limited to metallic films. The enhancement effect by EWAF can be demonstrated using dielectric films as well as metals.

The far field effects of EWAF enhancement will depend on illumination, opening size, EWAF spacing, and absorber thickness. An application that may likely be best suited for EWAF is contact holes, such as that shown in Figure 11.



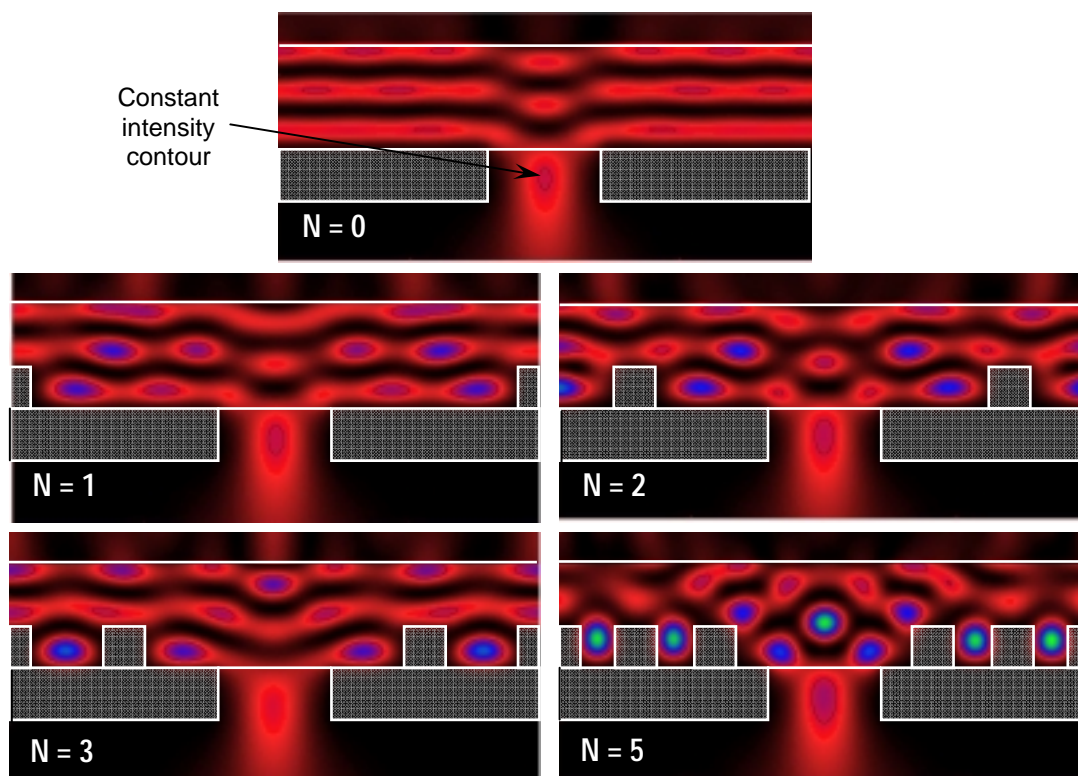


Figure 10. Near field impact of evanescent wave assist features on a 180nm opening in a chrome film (45nm at wafer) flanked by 62nm EWAFs at various densities. Wavelength is 193nm and the absorber film is a 90nm chromium film.

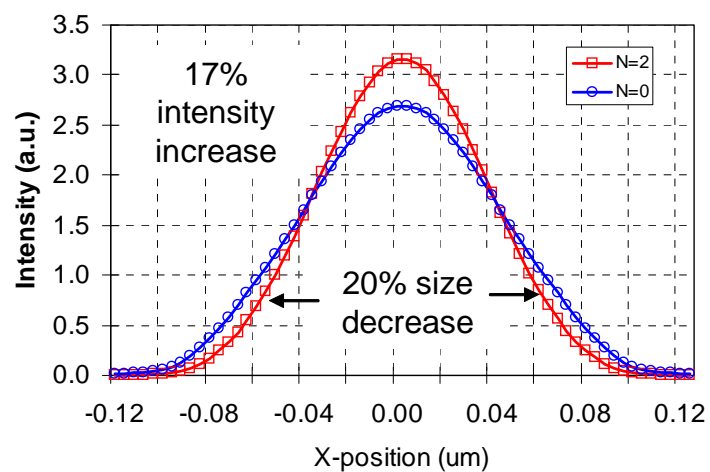


Figure 11. Intensity comparisons for the near field transmission through an opening with no EWAFs versus the optimum condition of flanking with two EWAFs.

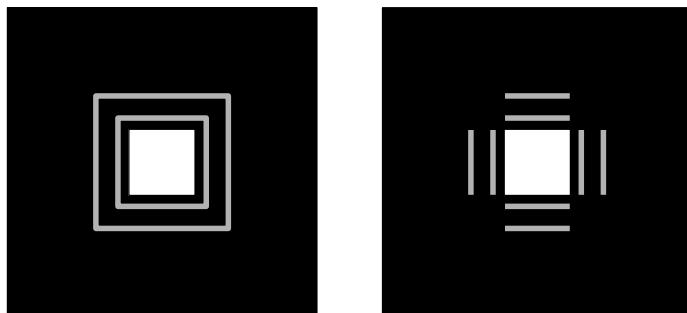


Figure 12. Example of EWAF for use with contact hole features, where the coupled evanescent effect can lead to enhancement across two directions.

## 6.0 CONCLUSIONS

As optical microlithography continues to be driven into sub-wavelength regimes, the importance of the energy that is evanescent at surface interfaces and near small openings becomes an interesting expansion of conventional imaging limited by diffraction. The true limits for optical lithography become more dependent upon materials and engineering challenges rather than on physics. We have demonstrated lithography at 193nm to  $0.13\lambda$  (26nm) at 1.85NA in image media with a refractive index lower than needed for propagation. This evanescent wave lithography (EWL) is a necessary technology for determining the limits of optical lithography in the sub-32nm range. Furthermore, through coupling of the evanescent wave effect at the mask plane, evanescent wave assist features (EWAF) provide for an opportunity to enhance imaging beyond that which is possible from the principles of diffraction alone.

## 7.0 REFERENCES

1. B. W. Smith, Y. Fan, M. Slocum, L. Zavyalova, Proc. SPIE Optical Microlithography, vol. 5754 (2005).
2. D. Kam, T. Milster, Optical Microlithography XVIII, Proc. SPIE Optical Microlithography, vol. 5754 (2005).
3. L.P. Ghislain, V.B. Elings, K.B. Crozier, S.R. Manalis, S.C. Minne, K. Wilder, G.S. Kino, C.F. Quate, Appl. Phys. Lett. 74, 501 (1999).
4. Q. Wu, G.D. Foke, R.D. Grober, L.P. Ghislain, Appl. Phys. Lett. 75, 4064 (1999).
5. M. Born and E. Wolf, *Principles of Optics*, Pergamon Press, Oxford, UK, 563, 1985.
6. B. W. Smith, D. E. Ewbank, SPIE Optical Microlithography XV, vol. 4691 (2002).
7. Born and Wolf, 638.
8. L. Salomon, F. de Fornel, J.P. Goudonnet, J. Opt. Soc. Am. A, 8, 2009 (1991).
9. P. Selenyi, Comp. Rend., 157, 1408 (1913).
10. S.M. Mansfield and G.S. Kino, Appl. Phys. Lett 57, 2615 (1990).
11. Y. Fan, A. Bourov, L. Zavyalova, J. Zhou, A. Estroff, N. Lafferty, B.W. Smith, Proc. SPIE Optical Microlithography, vol. 5754, (2005).
12. J. Sheats, B. Smith, *Microlithography: Science and Technology, Chapter 10: Multilayer Resists*, 1998.
13. Y. Leviatan, IEEE Trans. Microwave Theory and Techniques, 36, 1 (1988).
14. H. Lezec and T. Thio, Optics Express, 16, 3629 (2004).
15. Panoramic Technology Inc., Tempest PR2, 2006.